

Exploring Therapy Options with the Interactive Simulation of Intra-Aneurysmal Blood Flow on the GPU

Lars Walczak, Denis Fisseler, Frank Weichert

TU Dortmund, Computer Science VII, Otto-Hahn-Str. 16, 44149 Dortmund
{lars.walczak, denis.fisseler, frank.weichert}@tu-dortmund.de

Abstract: Occlusional performance of sole endoluminal stenting of intracranial aneurysms is controversially discussed in literature. Simulation of blood flow has been studied to shed light on possible causal attributions. The outcome however largely depends on various free parameters which all have considerable impact on simulation results. The current study is therefore conducted to find ways to define parameters and efficiently explore the huge parameter space with Lattice Boltzmann Methods on the GPU. A interactive simulation to assess flow and aneurysmal vorticity may result in a deeper understanding of blood flow and may also lead to more accurate information about factors that influence conditions for stenting of intracranial aneurysms. To analyse initial simulation results, simplifying models based on key features of MRI geometry and medical expert knowledge are used.

1 Introduction

The accurate incidence and prevalence of unruptured non-aortic aneurysms of 0.03cm or less in diameter is controversially discussed as the likelihood of detection is increasing with improved imaging techniques [JLN⁺09, LLW⁺11]. Size and perhaps geometry of the aneurysm are contributing to the risk of rupture (which may be less than 5% per year, [CSV11]). In the case of intracranial appearance, such rupture can cause devastating subarachnoid hemorrhage with high morbidity and mortality [MKS⁺10]. Unruptured aneurysms are therefore treated according to their location and patient's age. There is a selection of endovascular and surgery-based treatment modalities [Rin08].

During the last few years endovascular treatment of intracranial aneurysms was established as a possible minimal invasive alternative to neurosurgical therapy which was until then unequalled. The aneurysm is treated with electrolytically detachable coils, the use of which is limited for wide-necked aneurysms. Often it is not possible to coil an aneurysm after stent placement, so it would be preferable to treat the aneurysm with a covered or small-cell-designed stent that would permit an immediate occlusion. Quantitative approaches however applied to learn more about how specific design features of endovascular stents such as porosity, struts and mesh design affect intra-aneurysmal hemodynamics have mainly provided inconsistent results [KTTM08]. In some cases, stenting alone has been suggested to promote thrombogenic conditions such as reduced flow activity and prolonged stasis, and thereby occlude aneurysms simply by thrombosis.

But the selection of the preferred therapy is still controversially discussed, also in view of novel therapies, e.g. using flow dividers [KYGB11]. For this reason blood flow simulations in the context of aneurysms of elastotypic and/or mixtotypic arteries have been proposed [GJMS11, Yos06, Cha06], also in different studies, e.g. the ISAT study [MKS⁺02]. One of the most prominent ones is certainly the European Commission funded Aneurist Project¹. Their results [AML⁺09, CMWP11] state that a single simulation takes about 10 to 24 hours to complete. Imagine to test different stents models, different placements and orientations of the stent in the vessel. In a clinical situation, running times like these are of no direct use. Computer simulation-based therapy appears to be gaining acceptance in healthcare as several technical problems can be solved and facts be learnt away without animal experimentation or by working with actual patients. The speed with which considerable quantities of simulations can be performed may reduce the number of animal experiments and identify new issues to be covered.

The Lattice Boltzmann Method (LBM) is a popular mesoscopic method in computational fluid dynamics. It has been applied to a number of interesting flow problems including multi-phase and multi-component fluid flows [IOTK04, YS06, SC93]. A relatively simple single-phase, single-component flow represents a good candidate for exploring medical data sets. Fast execution times can be provided by using new programming paradigms for massively parallel processors like graphics processing units (GPUs) available in most medical workstations.

2 Simulation of Blood Flow

Among many different models a rather simple single-phase LBM is used to simulate blood flow. The following introduction to the method is very brief and the interested reader is referred to literature for further details. The monographs of [Suc01] or [ST06] are well known starting points.

2.1 Lattice Boltzmann Method

In continuum mechanics, fluid behaviour is described by time-varying density, velocity or pressure fields which corresponds to a macroscopic point of view. A microscopic point of view on the other hand would be to describe the motion of each atom or molecule. The LBM takes a mesoscopic approach: The (macroscopic) density ρ of a fluid is represented by multiple particle distribution functions (PDF). Each of these PDFs represent fluid particles which move in the same direction. The larger a PDF the more particles move into this direction. In the LBM, the continuous Boltzmann equation is discretised onto a regular three-dimensional lattice with a finite number of directions

$$\mathbf{e}_i = \begin{cases} c(\pm 1, 0, 0), c(0, \pm 1, 0), c(0, 0, \pm 1) & i = 1, \dots, 6 \\ c(\pm 1, \pm 1, 0), c(\pm 1, 0, \pm 1), c(0, \pm 1, \pm 1) & i = 7, \dots, 18 \end{cases} \quad (1)$$

¹aneurist project: www.aneurist.org

at each lattice node with corresponding PDFs f_i . The scalar value $c = \frac{\delta x}{\delta t}$ denotes the lattice speed and is based on grid (δx) and time (δt) resolution. The direction \mathbf{e}_0 is the zero-vector which represents particles at rest. Consequently, the model is called *D3Q19*. In two dimensions a *D2Q9* model with 9 discrete directions is used (details omitted). The evolution of the PDFs at each lattice node with regard to collisions between fluid particles is described by equation 2, which can be constructed by discretising the Boltzmann equation in time and space. It holds:

$$f_i(\mathbf{x} + \mathbf{e}_i, t + dt) - f_i(\mathbf{x}, t) = -\frac{f_i(\mathbf{x}, t) - f_i^{eq}(\mathbf{x}, t)}{\tau}, \quad i = 0, 1, \dots, 18 \quad (2)$$

in which

$$f_i^{eq} = w_i \rho \left(1 + \frac{3}{c^2} \mathbf{e}_i \cdot \mathbf{u} + \frac{9}{2c^4} (\mathbf{e}_i \cdot \mathbf{u})^2 - \frac{3}{2c^2} \mathbf{u} \cdot \mathbf{u} \right) \quad (3)$$

are the 19 equilibrium distribution functions and $w_0 = \frac{1}{3}$, $w_{1,\dots,6} = \frac{1}{18}$, $w_{7,\dots,18} = \frac{1}{36}$ are appropriate weighting factors. The evolution of the directional densities can be understood as a relaxation towards local equilibrium which is a function of the local density ρ , the current velocity \mathbf{u} and the relaxation time τ which is connected to the liquid viscosity $\nu = \frac{1}{3} (\tau - \frac{1}{2})$. The equilibrium distribution functions f_i^{eq} have the property to conserve mass. The density and velocity can be computed from the PDFs:

$$\rho(\mathbf{x}) = \sum_{i=0}^{18} f_i(\mathbf{x}), \quad \mathbf{u}(\mathbf{x}) = \frac{1}{\rho} \sum_{i=0}^{18} f_i(\mathbf{x}) \cdot \mathbf{e}_i. \quad (4)$$

Solid boundaries can relatively easily be incorporated by swapping opposite PDFs at solid nodes instead of performing the evolution based on equation 2. The evolution on solid nodes thus becomes $f_i(\mathbf{x} + \mathbf{e}_i, t + dt) = f_i^{opp}(\mathbf{x}, t)$, $i = 0, 1, \dots, 18$ with f_i^{opp} being the PDF in the opposite direction of \mathbf{e}_i . This technique known as bounce-back is one way of simulating the no-slip-condition at solid boundaries. Bounce-back is used at the blood vessel boundaries and the stents. The structures themselves are defined by multiple level sets.

A steady blood flow through the vessel is initiated by introducing pressure or velocity boundaries at the ends of the vessel. Here, velocity Dirichlet conditions at the inflow and velocity Neumann conditions at the outflow are applied. Those boundary conditions are applied on a macroscopic level (e.g. setting \mathbf{u}) as well as on a microscopic level (e.g. depending on \mathbf{u} , ρ and some of the f_i pointing into the fluid are set). See e.g. [ZH95] for further details. Pulsatile flows can be induced in a similar way by manipulating \mathbf{u} during the simulation. The compressibility error depends on the Mach number. With a Mach number $\ll 1$, the method is quasi incompressible. It has been shown in literature that the LBM approximates the time-dependent isothermal and incompressible Navier-Stokes Equations under this circumstance [JY03].

Due to the inherent parallelism of the LBM, where computation in each lattice node is only dependent on a local neighbourhood, the algorithm can be performed on highly-parallel computing architectures such as graphics processors and as such is suitable for interactive exploring of medical data sets. This approach has been taken in the reference implementation which uses OpenCL for computation. The two- or three-dimensional level set aneurysm and stent models can directly be used in both the CPU and GPU implementation.

2.2 Data Sets

For evaluation and comparison purposes a set of basic conditions are defined. These conditions have to be simple enough to allow the use of simplifying simulation models for faster access to initial simulation results, yet complex enough to model most aspects required for simulation of blood flow. Consequently our model consists of an incompressible fluid modelling and a suitable viscosity model. In addition, no-slip boundary conditions and an inflow velocity magnitude of $50 \frac{mm}{s}$ that is suitable for a small artery with a diameter of $1mm$ are applied. For the purpose of comparing the different simulation scenarios to each other an appropriate testing environment is needed. In addition to simulation domains generated directly from the MRI datasets, which sometimes suffer from irregularities and which are by concept limited to one stage in the formation process of an aneurysm, a synthetic aneurysm model, arbitrarily assumed to be similar to the terminal-type C morphology of unruptured aneurysms [OMH⁺08], was designed based on available MRI data and medical expert knowledge. As aneurysm development is currently not addressed in literature, three stages of aneurysm growth for the synthetic model are included in this study. The synthetic mesh facilitates the analysis of our physical modelling by providing level set volumes based on well structured 3D meshes for all required simulation domains. The cylindrical cross section of our synthetic model additionally simplifies the process of fitting experimental stents into the blood vessel and includes multiple stages in the formation process of the modelled aneurysm to allow further examination of the formation process.

3 Results

Based on available real geometry data of blood vessels featuring an aneurysm and our synthetic aneurysm models, some basic simulations are performed to compare the simulation scenarios. Lattice sizes are 272×384 and 128^3 respectively.

3.1 Aneurysm growth

To analyse aneurysm growth and its influence on flow dynamics, we perform some basic tests using the three stages of our synthetic aneurysm model. The velocity fields obtained with the models are shown in figures 1 and 2. The results from all simulation models share a parabolic velocity profile throughout the blood vessel, a drop in velocity magnitude near the opening of the aneurysm and a significant velocity magnitude at the aneurysm neck. The larger the aneurysm the higher the drop in magnitude in the vessel at the neck, cf. isoline velocity plot in figure 1. Comparing the converged results no such high velocity magnitudes do occur inside the aneurysm. On average the velocity magnitude is only $\approx 1 \frac{mm}{s}$ whereas in aneurysm neck the velocity is $\approx 14 - 20 \frac{mm}{s}$ depending on the scenario used (c.f. figure 3(c)).

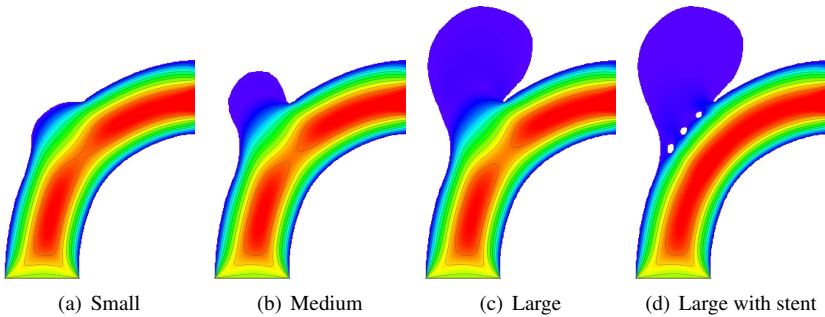


Figure 1: Visualization of 2D velocity field in a blood vessel near an aneurysm: **(a-c)** non-stented case and **(d)** with coarse stent.

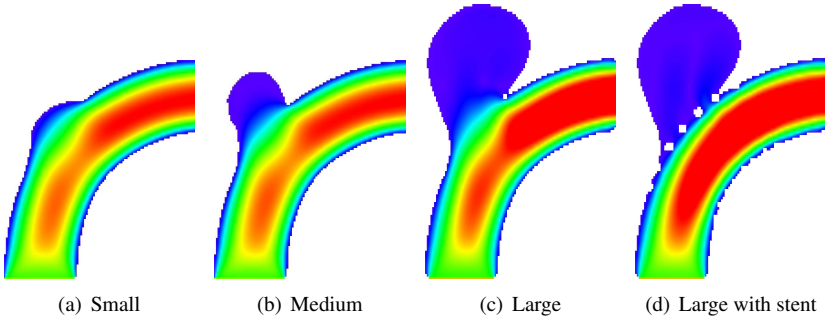


Figure 2: Visualization of a 2D cut through the 3D velocity field in a blood vessel near an aneurysm: **(a-c)** non-stented case and **(d)** with coarse stent.

3.2 Comparison with the Stented Case

To compare the stented vessel with its non-stented counterpart, we perform a series of simulations where 2D as well as 3D are evaluated. Colour coded velocity fields can be found in figures 1 as well as in figure 2. In figure 3, average and maximum flow velocity statistics of simulations are shown. It can be seen that much of the inflow at the aneurysm neck is effectively disabled by the stent. The average velocity inside the aneurysm drops from $\approx 1 \frac{mm}{s}$ in the non-stented case to $\approx 0.75 \frac{mm}{s}$. The flow behaviour of all simulations is nearly identical as the fluid streams from the vessel into the aneurysm lumen through the first three stent gaps and leaves the aneurysm sack through the fourth gap.

3.2.1 Stationary Flow

The converged results are ideal for comparison and analysis as they contain important flow information, c.f. figure 4. In figure 4(a) passively advected marker particles are used for vortex discovery in two dimensions. A vortex forms in the non-stented case above the aneurysm neck on the right side at position (75, 267). The vortex has a diameter of ≈ 56

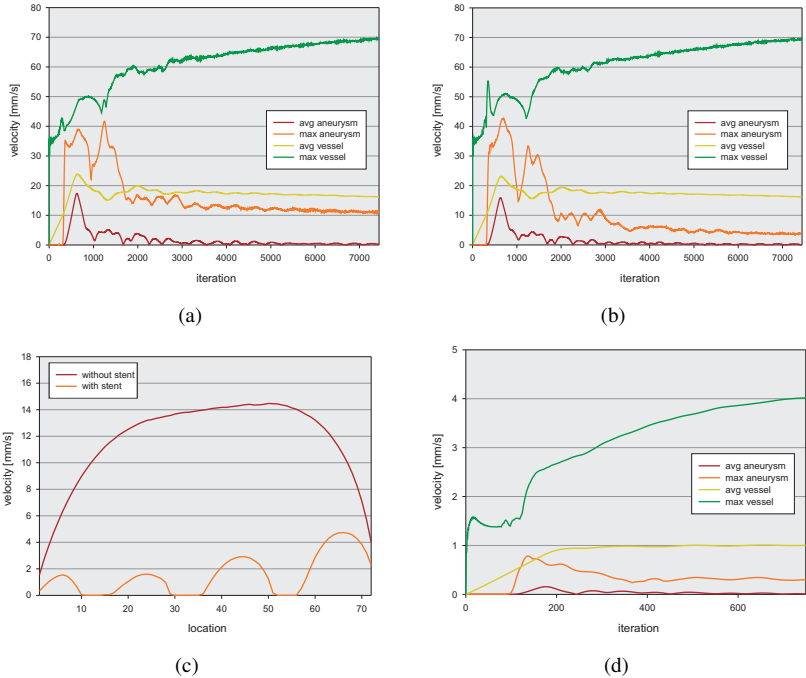


Figure 3: Flow statistics (average and maximum velocity) of the 2D simulation in the vessel and in the large aneurysm **(a)** non-stented case and **(b)** with coarse stent. **(c)** Converged stream profiles of the 2D simulation at the aneurysm neck with and without coarse stent. **(d)** Flow statistics (average and maximum velocity) of 3D simulations in the vessel and in the large aneurysm, stented case.

lattice units at its broadest side and rotates counter-clockwise. The rotational direction is reversed compared to the flow direction of the vessel. The isoline visualization in 4(b) shows a purple region at the same position (purple corresponds with zero velocity). The form of the vortex is not perfectly circular but is slightly deformed where it touches the vessel stream and reaches out into the aneurysm sack by which more rotational movement is induced. Two similar vortices with the same centre but a larger diameter can be found. These “secondary” vortices are ≈ 71 and 97 lattice units in size but of lower velocity magnitude compared to the primary vortex. Note that a smaller version of the primary vortex can already be found in the medium sized aneurysm experiment in figure 1(b). Compared to the stented case in figures 4(d) and 4(c) no such observations can be made. The purple regions in this case are only regions of almost zero velocity, the marker particles do not show a rotating behaviour. The velocity magnitude is much lower in the stented case.

Looking at the results of the 3D simulation (cf. figure 5(a)) a more complex behaviour than in 2D can be detected. Because of the symmetry of the synthetic data set the flow results are symmetric as well (in this case the symmetry occurs on the Z -axis). In the aneurysm four vortices can be discovered. The vortices are located off centre on the Z -axis. Two

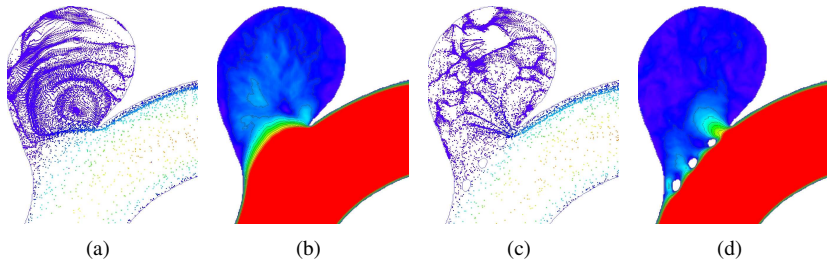


Figure 4: Vortex discovery with marker particles in a velocity field: **(a)** iso velocity field (non-stented case), **(b)** marker particles (non-stented case), **(c)** iso velocity field (non-stented case) and **(d)** marker particles (stented case).

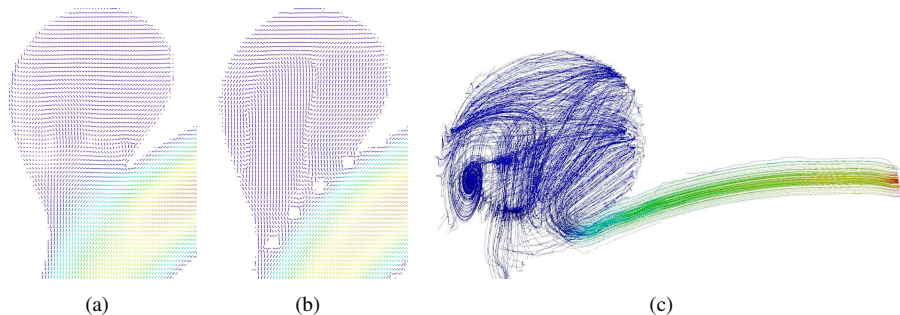


Figure 5: Flow behaviour in 3D: **(a)** non-stented case – two symmetric vortices occur on both sides of the y -axis and **(b)** stented case – downward upward downward flow movement inside the aneurysm. **(c)** 3D Streamline view of stented case: A broad vortex spans across the back of the aneurysm.

of these four vortices are located at the front of the aneurysm (greater X -axis values) near the outflow at the neck. In addition, two vortices are located at the back of the aneurysm, one third the way between neck and dome of the aneurysm on the Y -axis.

The 3D results (cf. figure 5(b)) of the stented case are more complex than the stented 2D case as well. A symmetric downward upward downward movement can be found inside the aneurysm lumen. The upward movement is induced by the inflow through the stent, down-flow on the right corresponds with outflow through the stent. The downward movement on the left ends at a broad vortex that is located in the back of the aneurysm and follows the arch of the geometry (cf. figure 5(c)) afterwards it mixes with the outflow stream. A zone of zero movement can be found on two sides, a possible area for thrombus growth.

3.2.2 Pulsatile Flow

In the time-dependent simulations additional flow information can be gained, e.g. from the flow behaviour through stent geometry. This is useful for analysing pulsatory behaviour in conjunction with the already modelled aspects. There is a inflow jet in the aneurysm lumen

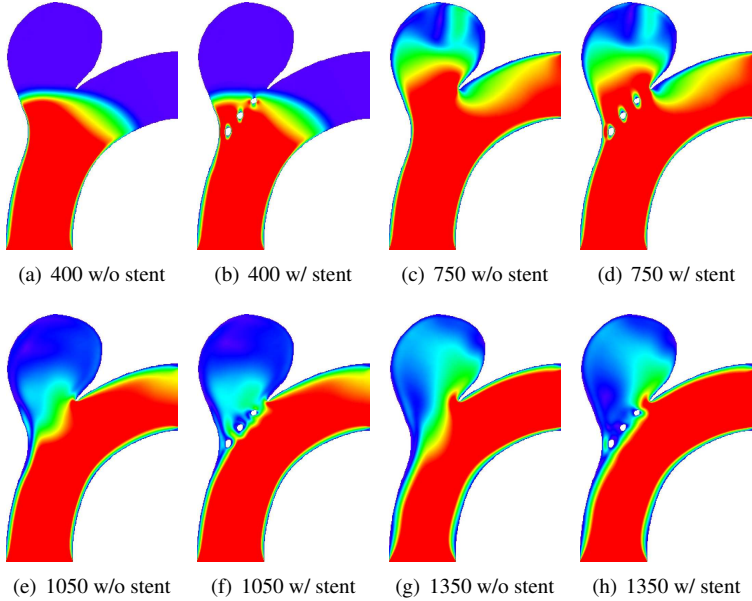


Figure 6: Visualisation of the velocity magnitude of the 2D simulation in the vessel and in the aneurysm at different time steps: (a), (c), (e) and (g), non-stented case and (b), (d), (f) and (h) with coarse stent. Colour scheme was chosen for maximum visibility inside the aneurysm lumen.

at the beginning of the flow process in both the stented and non-stented cases. Figure 3 shows the average and maximum velocity magnitude over time of the aneurysm as well as the average velocity in the vessel itself. In the stented case the flow is quickly slowed down after a certain time step (in the 2D case $t = 2,000$), but it has a higher maximum value compared with the non-stented case. Flow is suppressed even faster after time step $t = 1,600$ in the stentless case. The average curve however remains on a much higher level as flow is higher at the aneurysm neck. The graphs can be underlined with stills from the time-dependent simulation in figure 6 showing the colour coded velocity field at time steps "400", "750", "1,050" and "1,350" for both cases. The influence of this simple and coarse stent is more local as the overall pattern of the inflow jet matches during the first $1,600 - 2,000$ time steps. It can be seen that the jet reaches the dome of the aneurysm in both cases.

To get an idea how 2D simulation behaves near the stent, the converged 2D flows at the aneurysm neck in figure 3(c) are shown. The curves are taken at time step $t = 7,500$, note the impact of the application of a stent in front of the aneurysm neck after the inflow phase. The velocity magnitude drops from $\approx 14 \frac{mm}{s}$ in the non-stented case to $\approx 5 \frac{mm}{s}$ in the stented case at the neck.

3.3 Execution times

A straight forward OpenMP x86 implementation on a 2.93 Ghz intel Core i7 processor is outperformed by a factor of 130 – 200 with our OpenCL implementation on a nVidia GTX 560 Ti. With the above data sets 1225 and 84 frames per second can be reached in 2D repectively 3D. This perfomance gain is largely influenced by memory performance.

4 Discussion

The construct of mathematical representation of patient-specific anatomy is both feasible and applicable. A variety of practical issues has to be considered towards establishment of mathematical model-based tailor-made aneurysm therapy to realize personalized stenting for individual patients based on clinical and radiological findings.

In order to gain insights in the time-dependent flow process during a cardiac cycle LBM has proven to be a viable solution. The key conclusion is that the inflow phase into the aneurysm lumen during a cardiac cycle seems to be most interesting to analyse. The question of what influence do far reaching and concentrated inflow jets have on the integrity of the aneurysm sack has not been finally answered although some investigations have tried to [CMWP11]. The growth of aneurysms in conjunction with CFD has not been studied to date. Because of the runtime efficiency of the LBM, it seems possible to gain further insight in the complex flow processes of real geometry. A full 3D simulation is needed as indicated by the more complex results even in the simple synthetic case. The interactive frame rates of parallel LBM simulations can provide key simulation constellations.

The developed method has to be refined in a way that it provides the necessary resolution, respects pulsatory and material behaviour and models thrombosation to automatically find a stent geometry that is best for a specific situation. Further investigations are needed.

References

- [AML⁺09] S. Appanaboina, F. Mut, R. Löhner, C. Putman, and J. Cebral. Simulation of intracranial aneurysm stenting: techniques and challenges. *Comput. Methods Appl. Mech. Engrg.*, 198:3567–3582, 2009.
- [Cha06] H.S. Chang. Simulation of the natural history of cerebral aneurysms based on data from the International Study of Unruptured Intracranial Aneurysms. *J Neurosurg*, 104(2):188–94, 2006.
- [CMWP11] J. R. Cebral, F. Mut, J. Weir, and C. M. Putman. Association of hemodynamic characteristics and cerebral aneurysm rupture. *AJNR Am J Neuroradiol*, 32(2):264–270, 2011.
- [CSV11] A. Chien, J. Sayre, and F. Vintildeuela. Comparative Morphological Analysis of the Geometry of Ruptured and Unruptured Aneurysms. *Neurosurgery*, 69(2):349–356, 2011.

- [GJMS11] A. Gambaruto, J. Janela, A. Moura, and A. Sequeira. Sensitivity of hemodynamics in a patient specific cerebral aneurysm to vascular geometry and blood rheology. *Math Biosci Eng*, 8(2):409–423, 2011.
- [IOTK04] T. Inamuro, T. Ogata, S. Tajima, and N. Konishi. A lattice Boltzmann method for incompressible two-phase flows with large density differences. *Journal of Computational Physics*, 198(2):628–644, 2004.
- [JLN⁺09] S.W. Joo, S. Lee, S.J. Noh, Y.G. Jeong, M.S. Kim, and Y.T. Jeong. What Is the Significance of a Large Number of Ruptured Aneurysms Smaller than 7 mm in Diameter? *J Korean Neurosurg Soc*, 45(2):85–89, 2009.
- [JY03] M. Junk and W.-A. Yong. Rigorous Navier-Stokes Limit of the Lattice Boltzmann Equation. *Asymptotic Analysis*, 35:165–184, 2003.
- [KTTM08] M. Kim, D.B. Taulbee, M. Tremmel, and H. Meng. Comparison of two stents in modifying cerebral aneurysm hemodynamics. *Ann Biomed Eng*, 36:726–741, 2008.
- [KYGB11] M. Kamran, J. Yarnold, I.Q. Grunwald, and J.V. Byrne. Assessment of angiographic outcomes after flow diversion treatment of intracranial aneurysms: a new grading schema. *Neuroradiology*, 53(7):501–508, 2011.
- [LLW⁺11] J. Lu, J. Liu, L. Wang, P. Qi, and D. Wang. Tiny intracranial aneurysms: Endovascular treatment by coil embolisation or sole stent deployment. *Eur J Radiol*, 2011.
- [MKS⁺02] A. Molyneux, R. Kerr, I. Stratton, P. Sandercock, M. Clarke, J. Shrimpton, and R. Holman. International Subarachnoid Aneurysm Trial (ISAT) of neurosurgical clipping versus endovascular coiling in 2143 patients with ruptured intracranial aneurysms: a randomised trial. *Lancet*, 360(9342):1267–1274, 2002.
- [MKS⁺10] A. Morita, T. Kimura, M. Shojima, T. Sameshima, and T. Nishihara. Unruptured intracranial aneurysms: current perspectives on the origin and natural course, and quest for standards in the management strategy. *Neurol Med Chir (Tokyo)*, 50(9):777–87, 2010.
- [OMH⁺08] T. Ohshima, S. Miyachi, K.-I. Hattori, I. Takahashi, K. Ishii, T. Izumi, and J. Yoshida. Risk of aneurysmal rupture: the importance of neck orifice positioning-assessment using computational flow simulation. *Neurosurgery*, 62(4):767–773, 2008.
- [Rin08] G.J.E. Rinkel. Natural history, epidemiology and screening of unruptured intracranial aneurysms. *J Neuroradiol*, 35(2):99–103, 2008.
- [SC93] X. Shan and H. Chen. Lattice Boltzmann model for simulating flows with multiple phases and components. *Phys. Rev. E*, 47(3):1815–1819, Mar 1993.
- [ST06] M.C. Sukop and D.T. Thorne. *Lattice Boltzmann Modeling: An Introduction for Geoscientists and Engineers*. Springer, Heidelberg, Berlin, New York, 2006.
- [Suc01] S. Succi. *The lattice Boltzmann equation for fluid dynamics and beyond*. Clarendon Press Oxford University Press, Oxford New York, 2001.
- [Yos06] Y. Yoshimoto. A mathematical model of the natural history of intracranial aneurysms: quantification of the benefit of prophylactic treatment. *J Neurosurg*, 104(2):195–200, 2006.
- [YS06] P. Yuan and L. Schaefer. Equations of state in a lattice Boltzmann model. *Physics of Fluids*, 18, 2006.
- [ZH95] Q. Zou and X. He. On pressure and velocity flow boundary conditions for the lattice Boltzmann BGK model. *Biophysics*, 9:16, 1995.